Analytical and Computational Study of Unsteady Shock Motion on Hypersonic Forebodies

Mark J. Lewis,* Yvette Surline,† and John D. Anderson Jr.‡
University of Maryland, College Park, Maryland 20742

It is generally accepted that the design of hypersonic air-breathing transatmospheric vehicles will require relatively close matching of the position of the forebody bow shock, relative to the engine inlet cowl. Although it is likely that such matching can be accomplished for steady-state operation, an actual vehicle will be subject to unsteadiness and oscillations from a variety of sources. This work examines the behavior of a hypersonic bow shock subject to unsteady surface motions. In particular, the relative motion of a hypersonic bow shock is examined, subject to normal surface oscillations, for a wide range of frequencies. There are two analytical limits of response: a low-frequency, quasisteady regime where shock motion follows the surface perturbations; and a high-frequency, compression-expansion range where the finite disturbances generated by surface motions cancel out before reaching the shock. Computational solutions are presented that verify analytical results using a time-accurate inviscid MacCormack's scheme. The computation also provides solutions in the intermediate range of frequencies, demonstrating behavior such as shock curvature and phase shifts that are not discernible from the analytical limits. It is also shown that unsteadiness leads to time-varying profiles in thermodynamic properties, which may be of significance to the operation of a hypersonic engine.

Nomenclature

a = local speed of sound
C_P = specific heat at constant pressure
F = x-coordinate Euler vector
G = y-coordinate Euler vector
H = shock layer height
M = Mach number
p = pressure
R = gas constant
S = control volume surface
T = temperature
t = time variable
U = t-coordinate Euler vector
u = streamwise velocity
V = velocity
$\mathcal{V}$ = control volume
x = streamwise coordinate
y = normal coordinate
β = shock angle to flow
γ = ratio of specific heats
θ = surface angle to flow
ν = oscillation frequency
ρ = density
v = normal velocity
ω = circular frequency

Subscripts

i = x-direction grid coordinate
j = y-direction grid coordinate
1 = upstream
2 = downstream

Presented as Paper 90-0528 at the AIAA 28th Aerospace Sciences Meeting, Reno, NV, Jan. 8–11, 1990; received Jan. 29, 1990; revision received Sept. 5, 1990; accepted for publication Oct. 20, 1990. Copyright © 1990 by the American Institute of Aeronautics and Astronautics, Inc. All rights reserved.

*Assistant Professor, Department of Aerospace Engineering. Member AIAA.
†Graduate Research Fellow, Department of Aerospace Engineering. Student Member AIAA.
‡Professor, Department of Aerospace Engineering. Fellow AIAA.

Introduction

CURRENT plans for a transatmospheric vehicle depend on the design of weight-saving, engine-integrated airframes in which the external vehicle surfaces act as components of the propulsion system. In particular, the aircraft forebody would serve as the engine compression surface and the aftbody would act as the engine nozzle. The actual engine, which is envisioned to be a supersonic combustion ramjet, or scramjet, would actually be a high-speed combustion channel designed to operate in conjunction with the fore- and aftbodies. One of the implications of this integration is that the forebody must be properly shaped to provide efficient compression as an inlet and to satisfy the requirements of the hypersonic engine.

The design of the hypersonic forebody/inlet represents one of the fundamental hurdles that must be overcome if practical hypersonic vehicles are to be realized.[1] The performance of the inlet will be particularly critical because it must be relatively loss free to offset the penalties inherent in supersonic combustion. The combustor losses cannot be avoided because heat addition to a supersonic flow will always result in total pressure penalty, and so all other losses in the engine must be minimized.

Even worse, hypersonic engines will likely be operating at thrust-to-drag ratios close to unity, so that losses or excess drag due to improper inlet design may have a relatively large effect on net engine thrust. Since the fluid velocity increment through the hypersonic engine will be quite small compared to the flight velocity, on the order of 10% of freestream value at Mach 10, inlet losses or losses incurred further down the engine due to a poor inlet configuration can easily wipe out thrust gains in the combustor.

This work is motivated by the fact that control of the inlet bow shock, especially its location relative to the engine cowl lip, will be an important constraint in the design of an air-breathing hypersonic propulsion system. If the bow shock is placed too far away from the vehicle, below the engine cowl, there will be excessive wave drag. Because hypersonic vehicles will operate at thrust-to-drag ratios very close to unity, this additional cowl drag will be intolerable. Similarly, if the bow shock is swallowed into the cowl, deleterious reflections may propagate down through the engine. Therefore, it is likely that a hypersonic vehicle will have to fly with the bow shock approximately matched to the engine cowl.

It is not certain how accurate this matching should be; indeed, there is reason to suspect that exact matching of the shock onto the cowl is undesirable. In particular, recent experiments at Calspan[2] have dramatically demonstrated that the interaction of a bow shock with the cowl lip can produce a localized region of extremely high heating rate on the cowl surface. Even with active cooling, this elevated heating would probably burn through the cowl material. Therefore, it is likely that the shock will be best located with a slight offset from the cowl lip. However, it is also likely that the shock position must be controlled to prevent direct transient contact with the cowl and, thus, destructive heating. As an interesting aside, it is not known whether this shock interaction is a steady process. The experimental results are inconclusive on this point, and computational results have not been run with sufficient time durations to satisfactorily resolve this issue.[3]

A hypersonic inlet certainly can be designed so that, in the limit of steady operation, at a given design point, the forebody shock structure satisifies the cowl-matching criterion and provides the desired compression ahead of the combustion chamber.[4] However, it is not clear what the effect of unsteady phenomena will be on the inlet flowfield. It is likely that the vehicle wall will be oscillating due to aerodynamic unsteadiness, propulsion system oscillations, and acoustic disturbances. It is, therefore, of very strong interest to determine what these oscillations will do to the shock location, in as general a manner as possible.

The primary question to be addressed in this paper is the relative motion of the inlet bow shock at high Mach number under the influence of an oscillating wall and the resulting thermodynamic profiles on the inlet. Ideally, the shock should move exactly with the surface, so that when the vehicle experiences pitching oscillations, the forebody shock will move through exactly the same motion and thus remain fixed relative to the vehicle. Any difference in either the amplitude of that motion, or the phase of that motion, will result in displacement of the shock relative to the inlet surface. In fact, under certain conditions, there will be substantial departures from this behavior, and these departures will be examined both analytically and computationally.

This problem is depicted in Fig. 1. Motion of the forebody surface will drive the shock motion. If this shock motion is not identical to the surface motion, the location of the shock relative to the surface and the engine cowl will be varying. Because of the typical hypersonic shock angles, even small divergences of shock angle could result in large relative deflections. Note that both pitching and plunging motions are depicted.

Since transatmospheric vehicles have not yet been built, the likely oscillation frequencies for a hypersonic forebody are unknown. This work will consider driving frequency as a varying parameter and examine the shock and flowfield responses as a function of that frequency. No firm implication that any given oscillation frequency will be encountered in actual flight is implied. (Indeed, the noise levels associated with a scramjet are currently unknown, although one can imagine that such devices will be deafening!) The analytical solution is most applicable to solving at very low frequencies and very high frequencies; between these ranges, only the computational solution is available.

Analysis of Unsteady Behavior

Shock Motion in Low-Frequency Limit

An analytical solution of the shock motion subject to an oscillating wall has been presented in Ref. 4, based on a model developed by Ng.[5] The low-frequency scenario can be solved with a quasisteady model, in which time derivatives of density are neglected in the unsteady terms of the equations of fluid motion:

$$\frac{\partial \rho \mathcal{V}}{\partial t} \simeq \rho \frac{\partial \mathcal{V}}{\partial t} \tag{1}$$

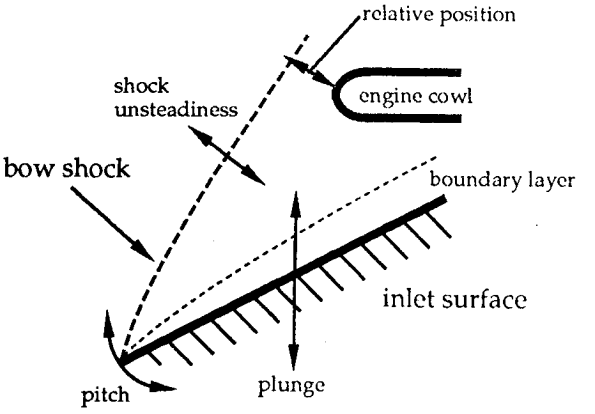

Fig. 1 Generic geometry for a hypersonic forebody showing shock location, pitching and plunging motion, and relative shock separation from cowl.

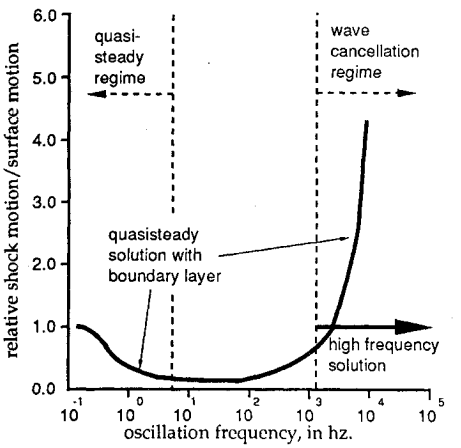

Fig. 2 Relative shock motion vs oscillation frequency. Quasisteady solution limit is calculated for a 1-m-thick downstream region between the shock and surface.

This quasisteady assumption thereby treats the moving shock as if it were a steady-state solution with constant velocity at each point in time. The surface motion is input as a steady downstream velocity boundary condition that must be satisfied at each point in time. Thus, the history of the shock motion is not important; if the downstream perturbation velocity is known at any moment, then the corresponding shock motion can be directly determined. This assumption restricts the resulting solution to low-frequency surface motions because, at higher frequencies, the time derivative of thermodynamic properties will become large. The range of application of the quasisteady assumption can be verified with a self-consistency calculation on the thermodynamic time derivatives and by comparing to the computational model. The steady-state shock relations can then be applied at each point in time.[6]

The quasisteady solution can be presented on a plot of relative shock motion as a function of surface oscillation frequency for fixed values of oscillation amplitude. Figure 2 is a typical representation of the extremes of shock motion relative to the surface motion, at conditions corresponding to a wedge of 5 deg flying at Mach 20, 50 km, with a 1-cm oscillation amplitude. In the limit of zero oscillating frequency, the downstream oscillation velocity approaches zero, and thus the moving surface can have no effect on the shock, and so the relative motion is just that surface motion. Observe that the shock motion matches the surface motion even at relatively low frequencies, implying that, throughout most of the frequency range, the shock is approximately fixed relative to the surface.

The quasisteady model can be modified to include the presence of a boundary layer, as shown in Ref. 4, which incorporated the model of Bertram and Blackstock[7] to couple boundary-layer thickness with shock pressure ratio. At low frequencies, the boundary layer has no effect on the motion of the shock. However, at high frequencies, the quasisteady model predicts that the boundary layer thickness can be coupled to the pressure variations induced by the initial shock oscillation, thereby amplifying the apparent surface motion. However, this amplification is predicted in the quasisteady model at frequencies well above the range of applicability of the quasisteady assumptions, as presented in Fig. 2.

Inviscid Shock Motion in High-Frequency Limit

The quasisteady assumption is only valid at low frequencies; at higher frequencies, the time derivatives of thermodynamic properties will become important. For control volume height of a few meters, and conditions typical of a hypersonic inlet flow, there is a cutoff in the applicability of the quasisteady model in the neighborhood of 10–30 Hz, as found in Ref. 4.

Although the frequency range above the quasisteady regime must be handled with the complete unsteady equations, some simplifications can be drawn for extremely high frequencies. In the quasisteady range, continuity is satisfied in the presence of surface motion by moving the shock, whereas the instantaneous values of density remain unchanged. The quasisteady assumption fails when the downstream region experiences large order density changes to satisfy continuity requirements. In the limit of high frequency, this density change will accommodate all of the plate motion, and the shock will remain stationary. In this case,

$$\frac{\partial \rho \nabla}{\partial t} \simeq \nabla \frac{\partial \rho}{\partial t} \tag{2}$$

This high-frequency regime can best be understood with the one-dimensional piston analogy. An oscillating piston that generates a finite compression wave as it moves into the gas generates a finite expansion, or rarefaction wave, as it withdraws. The expansion wave will catch up with the compression wave and weaken it, eventually canceling it if the piston motion is symmetrical.[8] The highest frequency surface motion that can drive the shock corresponds to the point where compression waves generated by the oscillating surface are canceled by subsequent rarefaction waves before they reach the shock, and so the shock is not affected by the surface motion.

For the conditions of Fig. 2, cancellation occurs beneath the shock at a minimum frequency of about 1 kHz, above which the shock will presumably remain fixed even in the presence of surface motions. Between about 10 Hz and 1 kHz, neither model is applicable and the computational solution must be depended on.

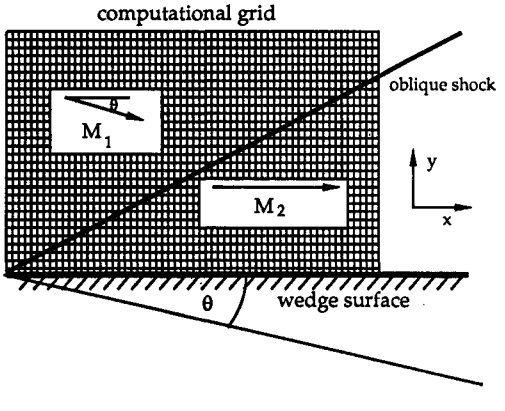

Fig. 3 Physical and computational plane.

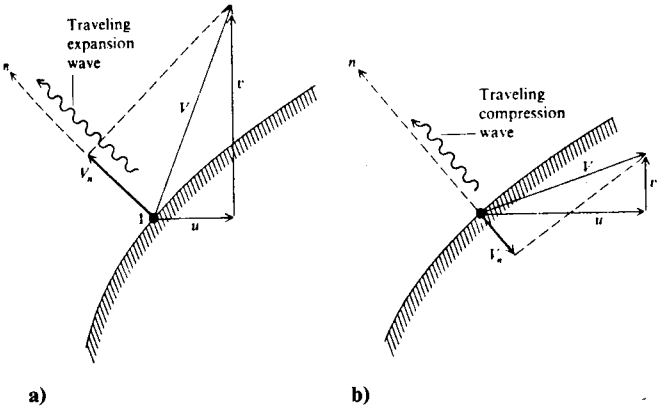

Fig. 4 Illustration of the boundary condition of the wall: a) traveling expansion wave; b) traveling compression wave.

Computational Solution

The two-dimensional, compressible, unsteady Euler equations are solved by means of a time-dependent finite difference approach that incorporates MacCormack's original explicit algorithm, which is simple to implement and is second-order accurate in both time and space. MacCormack's time-explicit scheme involves marching the solution of the governing equations by numerically differencing the equations twice at each time step in a predictor-corrector fashion. In the predictor step, a first-order forward difference is used to evaluate the spatial derivative using the known values of the flowfield at time t. These spatial derivatives are then substituted into a first-order Taylor series in time to calculate the predicted values for the flowfield properties at time t^*.

Using the predicted values of the flowfield, the corrector step is implemented by recomputing the time derivatives using first-order rearward differences for the spatial derivatives. The average value of the predicted and corrected derivatives is then substituted into the Taylor series time expansion to evaluate properties at time $t + \Delta t$. This has a net result of being equivalent to a second-order accurate central difference approximation. The averaging of spatial derivatives at time $t = n$ and time $t = n + 1$ effectively centers the method in time and ensures second-order accuracy.

Emphasis is placed on the scheme's time accuracy since it is the unsteady flowfield generated by the oscillating wedge and the corresponding oscillation of the oblique shock wave that is of interest in this problem. MacCormack's method has traditionally been used on the unsteady equations to solve mixed flowfield problems where the steady-state solution is obtained in the asymptotic limit of large times. In this case, it is the transient flowfield that is of interest.

Computational Procedure

The physical and computational space for flow past a wedge are identical if the coordinates of the physical space are oriented parallel and normal to the surface of the wedge (see Fig. 3). The result is a rectangular grid where MacCormack's technique can be applied, with the half-angle of the wedge set by adjusting the direction of the incoming freestream flow relative to the body-oriented coordinate system. MacCormack's predictor-corrector scheme was applied to the internal grid points with the addition of artificial viscosity in order to capture the shock wave with minimal oscillations. More will be said about artificial viscosity at the end of this section. The code was initially used to obtain the steady-state solution for flow over a wedge. Once the steady-state solution was obtained, i.e., the shock wave well established and in agreement with oblique shock-wave theory, the wedge was oscillated according to a specified sinusoidal input, and results were obtained for the transient behavior of the resulting shock-wave motion.

Boundary Conditions

Inflow Boundaries

The inflow consisted of a supersonic freestream of specified magnitude and direction that was held constant with time. The pressure and temperature were also set at the appropriate freestream values. The inflow conditions for all test cases were the steady-state solutions used to validate the code.

Downstream Boundaries

The shock wave generated in the flowfield for all cases was oblique with very shallow angle, and, thus, the flow for all cases downstream of the shock was supersonic. The properties of the flowfield at the downstream boundary was obtained by first-order linear extrapolation.

Wall Boundaries

The boundary condition along the body was the usual inviscid flow condition: the velocity must be tangent to the surface ($\boldsymbol{v} \cdot \boldsymbol{n} = 0$, where $\boldsymbol{n}$ is the unit vector normal to the surface). In order to implement this boundary condition, the velocity, along with the remaining flowfield variables, were calculated first with MacCormack's technique using forward differences in both the predictor and corrector steps. In general, the value of velocity so obtained will violate the preceding condition. In other words, if we consider the y component of velocity v, it will not in general equal the y component velocity of the specified plate motion; it was, therefore, necessary to set $v = v_{\text{plate}}$ to satisfy the flow tangency condition.

To accomplish this, a local, finite, one-dimensional, isentropic expansion or compression wave was sent away from the surface into the flow of sufficient strength to equilibrate the v velocity of the flow with that of the plate motion, as shown in Fig. 4. When the steady-state solution was calculated, the normal velocity of the plate was set equal to zero. A sinusoidal motion was input for the plate:

$$y_{\text{plate}} = A \sin\omega t \tag{3a}$$

$$v_{\text{plate}} = v_{\max} \cos\omega t \tag{3b}$$

where $v_{\max} = \omega A$. This motion is normal to the wedge surface, and so it is not exactly pure plunge as defined in Fig. 1. The local expansion and compression waves changed the computed values of temperature and pressure in the following way:

$$T_{\text{new}} = \frac{1}{\gamma R}\left(\frac{\gamma - 1}{2}\left[\, v_{\text{plate}} - J_- \right]\right)^2 \tag{4}$$

where J_- is a Reimann invariant, $J_- = v_{\text{old}} - 2a/(\gamma - 1)$, and

$$\frac{p_{\text{new}}}{p_{\text{old}}} = \left(\frac{T_{\text{new}}}{T_{\text{old}}}\right)^{\frac{\gamma}{\gamma - 1}} \tag{5}$$

In Eq. (5), T_{old}, P_{old}, and v_{old} are the values obtained from one-sided differencing, and p_{new} is obtained from the isentropic relationship to the temperature. This procedure is a modification of one that was described by Anderson.[10]

Table 1 Unsteady wedge motion test cases, $\theta = 6.44$ deg

M	ν, Hz	Amplitude, m
1	1	0.5
10	1	0.1
	10	0.1
	10	0.5
	100	0.1
20	10	0.01
	100	0.01
	100	0.1
	1000	0.01
	1000	0.01
	500	0.01

Artificial Viscosity

Artificial viscosity was added to the scheme in order to stabilize it and capture shock waves with high resolution and minimal oscillations. The type of dissipation that was used was a fourth-order damping term that was added to the right side of the predictor and corrector equation:

$$\begin{aligned}\Delta U_{ij} = {} & C_x\left(\frac{p_{i+1,j} - 2p_{i,j} + p_{i-1,j}}{p_{i+1,j} + 2p_{i,j} + p_{i-1,j}}\right) \\ & \times (U_{i+1,j} - 2U_{i,j} + U_{i-1,j})(|u_{i,j}| + a_{i,j})\frac{\Delta t}{\Delta x} \\ & + C_y\left(\frac{p_{i,j+1} - 2p_{i,j} + p_{i,j-1}}{p_{i,j+1} + 2p_{i,j} + p_{i,j-1}}\right) \\ & \times (U_{i,j+1} - 2U_{i,j} + U_{i,j-1})(|v_{i,j}| + a_{i,j})\frac{\Delta t}{\Delta y}\end{aligned} \tag{6}$$

$$U_{i,j}^{n+1} = U_{i,j}^{n} + \left(\frac{\partial U^*}{\partial t}\right)_{\text{average}} \Delta t + \Delta U_{i,j} \tag{7}$$

where C_x and C_y are two assigned constants. For viscous flows around compression corners,[11] C_x and C_y range in value between 0.0 and 0.5; however, since the Euler equations have no inherent dissipation, larger values were used to smooth out the pre- and postshock oscillations. All calculations were carried out with $C_x = C_y = 3.0$. Several cases were run with varying artificial viscosity, from which it was determined that artificial viscosity had no effect on the defined shock location, merely serving to capture the shock with higher resolution.

Code Validation

In order to validate the code and infer the influence of the artificial viscosity, solutions for various wedge angles and Mach numbers, from low supersonic to high hypersonic, were obtained in the steady state. In all cases, the pressure profiles matched the predictions from oblique shock theory to within a few percent of the actual solution, the worst being approximately 5% error for a strong shock at Mach 5, $\theta = 18$ deg. Additionally, the shocks that were generated were highly resolved with minimal pre- and postshock oscillations. From this, it was concluded that the amount of artificial viscosity added to the scheme did not invalidate the results with numerical smearing.

In all cases, the steady-state solution displayed an entropy layer close to the wall across less than 8% of the grid, in which both the temperature and u velocity displayed sharp gradients. This layer remained confined, as indicated by its uniform thickness along the plate, and it had no normal pressure gradient. Outside the entropy layer, flow conditions corresponded exactly to the oblique shock solutions. Such entropy layers are typical of flowfields with curved shock waves. In the present case, this behavior can be attributed to a combination of two effects:

1) At the leading edge of the plate, the shock is slightly curved. This is due to the calculation of properties in this region because of the strong influence of the fixed inflow boundary conditions and the wall boundary adjustments on the internal grid points.

2) Treatment of the normal component of velocity comes out of a one-dimensional unsteady characteristics solution. Thus, adjustments in u velocity to enforce flow tangency are neglected and only the v component of velocity is adjusted. It is assumed that the adjustment in temperature that follows that of v velocity acts in such a way as to adequately account for the change in kinetic energy; however, this may not be the case and this energy imbalance may manifest itself as a type of entropy layer.

In fact, the presence of an entropy layer, which is fundamentally boundary-layerlike, seemed to confirm the expectations that a boundary layer would have little impact on the behavior of the inviscid flowfield, as the pressure near the wall corresponded to the correct value from oblique shock-wave theory. The entropy layer did not respond to the wall motions, just as it is expected that a boundary layer would be insensitive in the motion range of interest.

Test Cases

Steady-state solutions were obtained first for several representative conditions. These converged cases were used as initial conditions for the unsteady wedge problem, which was run at Mach 5, 10, 15, and 20 and at wedge angle $\theta = 6.44$ deg. This particular wedge angle was selected to represent a typical hypersonic forebody with a 4:1 static pressure rise at design Mach number 10. In addition, tests were run at Mach 2 with no wedge angle and at Mach 5 with an 18-deg wedge angle, the latter of which was selected to generate a relatively strong shock with angle $\beta = 30$ deg. The choice of absolute value of thermodynamic conditions for these tests was somewhat arbitrary because it is only the ratios across the shock that are of importance. Unsteady test cases were run at very low and very high frequencies and were seen to reproduce the analytical results explained earlier. Table 1 lists the various run conditions that were chosen.

For each calculation, a 31×61 grid was used. This was sufficient to locate the shock with the desired precision, yet was coarse enough that run times were of reasonably short duration. The actual physical dimensions of the grid varied in the y direction between 6.0 m at Mach 5 and 2.1 m at Mach 20. The physical grid length was 30 m in all cases. All pressure profiles and data on shock location were obtained at a position 27 m down from the leading edge of the plate. This grid length was chosen as representative of a hypersonic forebody on a transatmospheric air-breathing hypersonic vehicle. A downstream location was chosen for the analysis because of the importance of adequately modeling the flowfield as it enters the engine of this type of vehicle.

Measurement of Shock Location

For most of the results, the parameter of primary interest was shock location. In the code, a shock capturing method was used that caused the shock to be smeared over approximately five grid points in each case. To pinpoint shock location at a given x position ($x = 27$ m was used in all cases to represent the end of a 30-m long inlet forebody), pressure profiles were obtained and the shock location was set at the

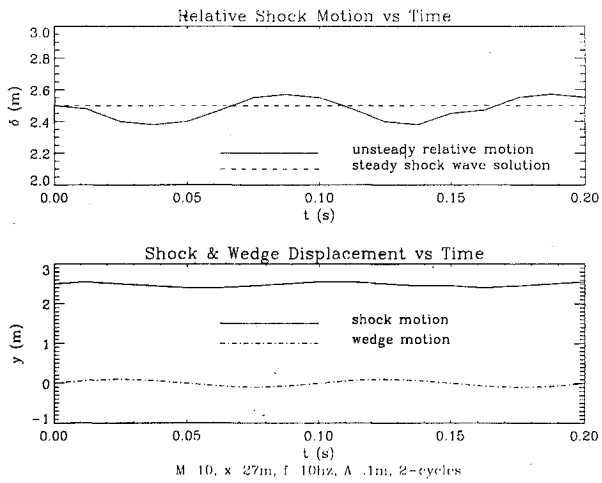

Fig. 5 Unsteady wedge flow at $M = 10$, $\nu = 10$ Hz, amplitude = 0.1 m: a) relative shock motion vs time; b) shock and wedge displacement vs time.

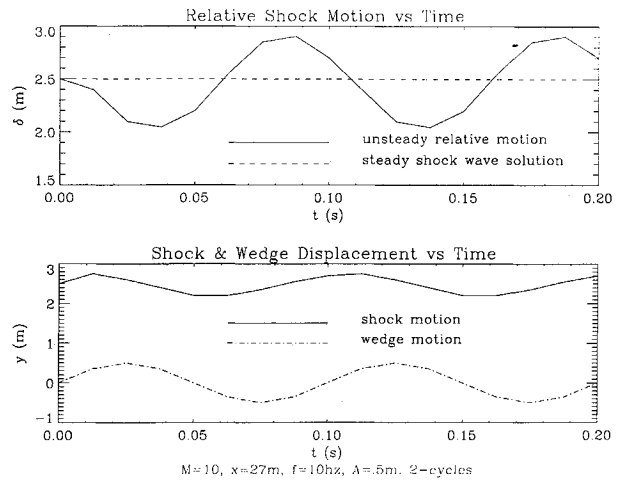

Fig. 6 Unsteady wedge flow at $M = 10$, $\nu = 10$ Hz, amplitude = 0.5 m: a) relative shock motion vs time; b) shock and wedge displacement vs time.

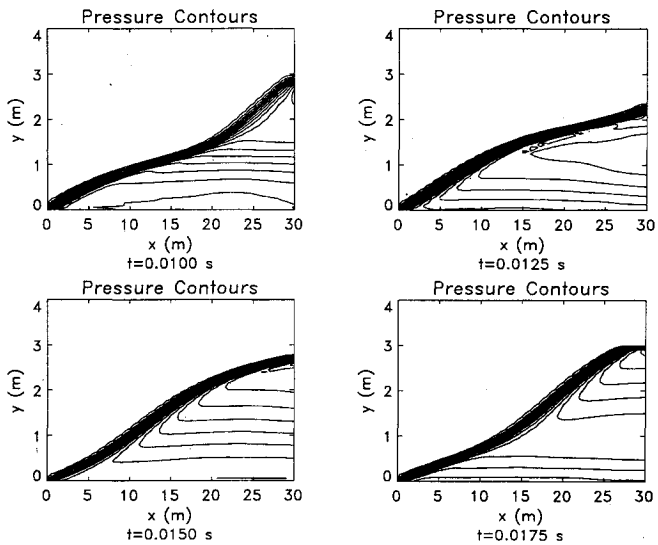

Fig. 7 Shock curvature for 1 cycle, $M = 10$, $\nu = 100$ Hz, amplitude = 0.1 m. Shown are 30 evenly spaced pressure contours, ratio of maximum to minimum contour = 5: a) $t = 0.0100$ s; b) $t = 0.0150$ s; c) $t = 0.0125$ s; d) $t = 0.0175$ s.

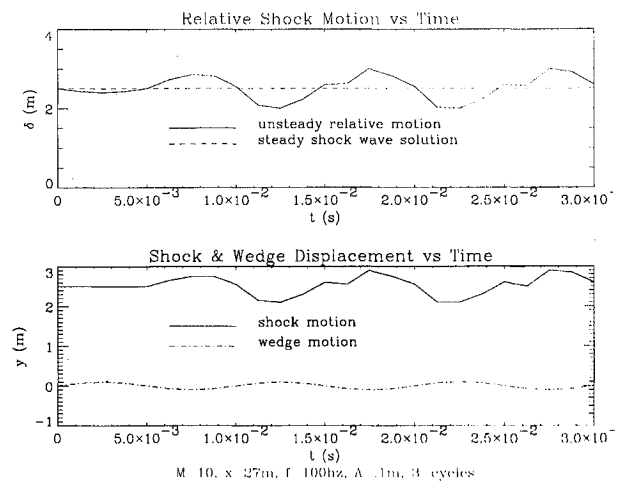

Fig. 8 Unsteady wedge flow at $M = 10$, $\nu = 100$ Hz, amplitude = 0.1 m: a) relative shock motion vs time; b) shock and wedge displacement vs time.

inflection point of the flattened region over which the shock was spread. In this manner, the shock location was measured with consistency for each case. Solutions were run with much less artificial viscosity, from which it was determined that artificial viscosity had no effect on the location of the shock inflection point.

Limitations of the Code

There are inherent limitations on the performance of the algorithm chosen along with the imposed boundary conditions. These include the following:

1) The wedge surface does not actually move in the computational domain. This restricts the motion that was studied to small amplitudes, especially at the leading edge where shock attachment may be an issue.

2) The locally one-dimensional boundary condition on the normal component of velocity does affect the calculation of temperature and normal velocity at the wall. This could have some consequences on the calculation of the unsteady behavior of the shock wave.

3) Artificial viscosity was relatively high because shock definition was important in this study. In fact, less artificial viscosity might have been required overall if it had been decreased as the shock wave was beginning to form. Future work may include this correction.

4) The existing code cannot handle high surface velocities, limiting high-frequency results to modest amplitudes.

5) The solution given here does not include the effects of viscosity. It would be interesting to note the type of interaction the boundary layer would have had with the shock movement; this also remains a topic for future work.

Results

In the first series of cases, the surface was oscillated at low frequency and the shock behavior for various Mach numbers and amplitudes was recorded. It was found that, for frequencies of 1 Hz, the shock did not move relative to the plate surface. This was true for Mach 5 at 0.5-m amplitude and Mach 10 at 0.1-m amplitude. In both cases, the actual input velocity of the plate was minimal, ranging from 0.6 to 3 m/s. This exactly reproduced the results of the analytical solution because a very small perturbation velocity will have a correspondingly small effect on the shock position, as indicated in Fig. 2.

At a slightly higher frequency of 10 Hz, a Mach 10 wedge flow was oscillated at amplitudes of 0.1 and 0.5 m. It was found that the resulting motion of the shock wave was cyclic and slightly out of phase with the surface motion. This can be seen in Figs. 5 and 6 for each case, respectively. Figures 5 and 6 also show the relative shock motion over two cycles for each of the two amplitudes. The maximum and minimum relative displacements were found to be approximately equal to the input amplitude, again exactly matching the predictions of the low-frequency analysis.

In the second series of test cases, the surface was oscillated at an intermediate frequency of 100 Hz for various Mach numbers and amplitudes. In the first case, Mach 10 wedge flow was used as the initial condition for a 0.1-m amplitude oscillation. The results show several interesting features that are beyond the limits of the analytical solution. One important characteristic is that the shock wave is curved. The shock tends to curve downstream of the leading edge of the plate, with an inflection point developing within a few meters and traveling downstream with time at speeds in excess of the flow velocity (which is not surprising since compression and expansion waves are traveling obliquely to the shock). The shape of the shock at various points in the cycle is given in Fig. 7. The shock curvature was also found to be repeatable from cycle to cycle. Both input surface motion and resulting shock motion vs time can be found in Fig. 8, along with the resulting relative motion.

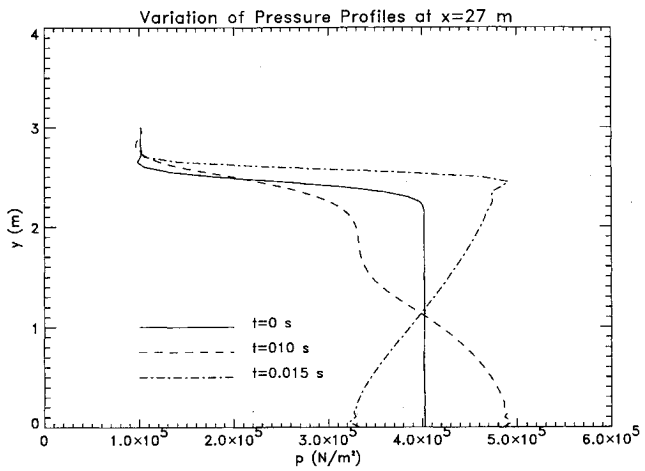

Fig. 9 Comparison of pressure profiles for $M = 10$, $\nu = 100$ Hz, amplitude = 0.1 m.

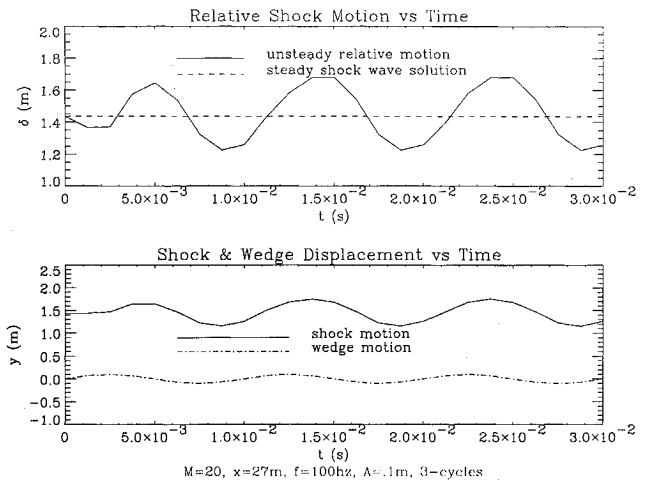

Fig. 10 Unsteady wedge flow at $M = 20$, $\nu = 100$ Hz, amplitude = 0.1 m: a) relative shock motion vs time; b) shock and wedge displacement vs time.

In this case, the maximum and minimum displacement of the shock wave has increased by a factor of 5 over the input amplitude of 0.1 m. This large magnification of motion had notable consequences on the pressure field behind the shock wave, which is no longer uniform. At the wall, the pressure varied by more than ± 0.75 atm, approximately 36% of the steady-state value. This variation in pressure can be seen in Fig. 9, which contrasts pressure profiles occurring at minimum wall pressure and maximum wall pressure with the theoretical steady shock-wave solution. A similar case was run with Mach 20 wedge flow, all other parameters being the same. The same characteristics appeared as observed in the Mach 10 flow, but with less severity. The relative shock displacement at maximum and minimum values increased by a factor of approximately 3. This can be seen in Fig. 10.

To demonstrate the influence of amplitude on the middle frequencies, a case with $M = 20$, $\nu = 100$ Hz, and amplitude of 0.01 m was run. It was found that the shock remained stationary. This suggests that the phenomenon of shock curvature is sensitive to amplitude as well as frequency, which is not surprising since wall velocity is proportional to both.

In the final series of test cases, the surface was oscillated at higher frequencies of 1000 and 5000 Hz for Mach 20 wedge flow. The shock wave did not move in either the 1000- or 5000-Hz frequency cases. This can be observed in Fig. 11. At these high frequencies, cancellation of expansion and compression waves occur below the shock wave such that the shock is uneffected by the wedge motion. In contrasting the

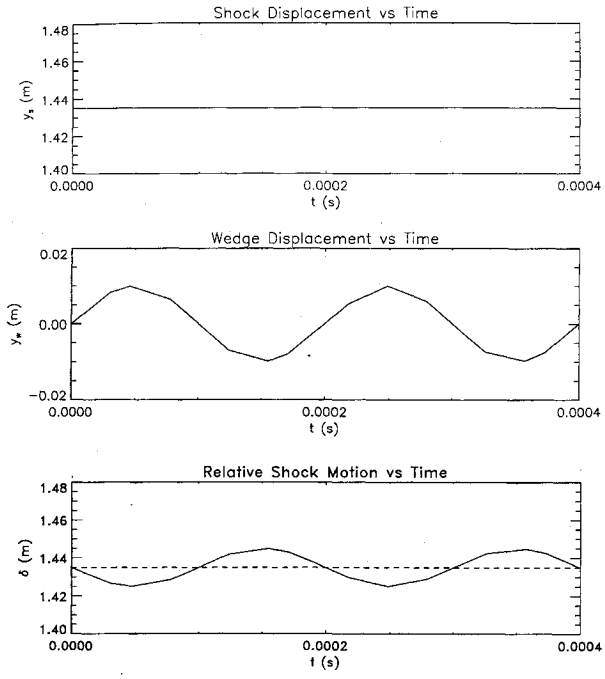

Fig. 11 Unsteady wedge flow at $M = 20$, $\nu = 5000$ Hz, amplitude = 0.01 m: a) shock displacement vs time; b) wedge displacement vs time; c) relative shock motion vs time.

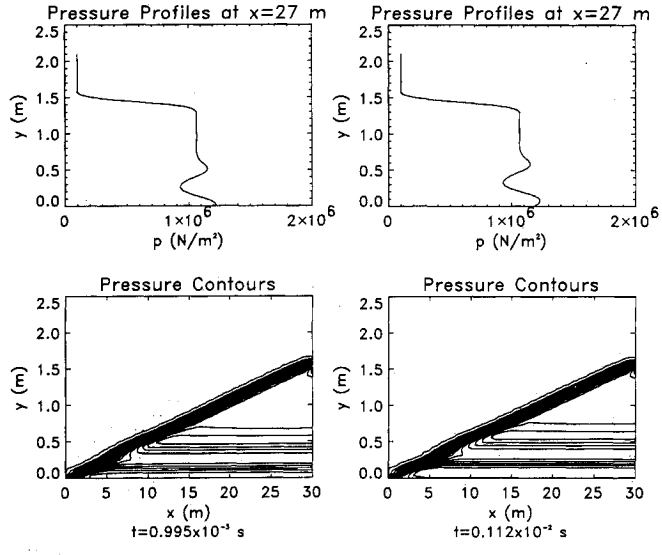

Fig. 12 Dissipation of wall disturbance at $\nu = 1000$ Hz. Shown are 30 evenly spaced pressure contours, ratio of maximum to minimum contour = 5.

two frequencies, it was found that the characteristic length for wave cancellation was considerably smaller for the higher frequency. This is in direct agreement with the analytical model and can be seen in Fig. 12. To see the effect of amplitude, a case was run at 1000-Hz frequency and 0.001-m amplitude. Similar characteristics were observed suggesting that, at the higher frequencies, the shock response is relatively insensitive to amplitude.

Conclusions

Low-frequency vibration corresponding to frequencies of approximately 10 Hz, at amplitudes on the order of 0.1 m, tend to produce a linear shock displacement response. In general, the shock and surface will not be in phase, but the relative motion will be limited to the amplitude of the surface motion. At frequencies lower than this, the frequency and amplitude combination will produce surface motion that is too slight to disturb the shock wave from its steady-state position.

At high frequency, the expansion waves and compression waves generated by the movement of the surface tend to cancel in a characteristic length that is less than the height of the shock such that the shock is not disturbed from its position. Closer to the leading edge, where the shock sits closer to the surface, the cancellation length is equal to the shock-wave height and the shock wave is bent. This curvature is localized to a small region, and locations downstream of that are not affected. Also, at high frequencies, the resulting behavior of the shock wave is largely insensitive to amplitude.

Midrange frequency vibration exhibits the interesting feature of shock curvature. Here, the expansion and compression waves that result from the plate movement interact with the shock and strongly affect the shock location. The curvature of the shock wave induces a flowfield downstream of the shock that is far from uniform, and, thus, the pressure behind the shock is not uniform. Wall pressures had the highest fluctuation with pressure ranging by more than 1.5 atm. Both the nonuniformity of the pressure field and the timewise fluctuation of pressure can have serious consequences on engine performance since reaction times for combustion are very sensitive to pressure.[12] Therefore, these oscillations can have a very profound effect on engine performance since the engine will see pressure fluctuations with time and dramatic flow nonuniformities.[13,14] Even worse, it is possible that these oscillations could produce reinforcing perturbations in engine performance and thus pose a serious hazard to vehicle operation.

Overall, shock motion, though decidedly nonlinear, resembles the motion of a simple harmonic oscillator. At low frequencies, shock amplitude is the driving amplitude; at some middle range, a resonance of sorts is reached and the amplitude is substantially greater than the driving motion. Finally, at the highest frequencies, there is attenuation of the driving function. This analogy should be applied with caution since the driving mechanism is nonlinear and the mass of the driven system is changing along the plate.

In all cases, the effect of the wedge oscillation was lessened with increasing Mach number. This was to be expected since, at higher Mach numbers, the bulk inertia of the flow dominates over the small velocity of the plate induced by the plate motion.

Future work will address some of the deficiencies outlined earlier. In particular, an actual moving wall, as opposed to a simple imposed velocity field, will be added. Viscous effects will also be added. This may be particularly significant in the middle frequency range, where large scale oscillations in pressure were observed. It will be of particular interest to observe the coupling between a boundary-layer profile and the profile imposed by unsteady behavior.

Acknowledgments

A portion of this work was supported by the Charles Stark Draper Laboratory under Contract DL-H-261843, supervised by Phil Hattis. The authors would like to thank Spyridon Lekoudis of the Office of Naval Research and Ugo Piomelli of the Department of Mechanical Engineering at the University of Maryland for their help in developing the computational solution. Charles Lind and James Weber of the Department of Aerospace Engineering at the University of Maryland also provided assistance in the preparation of this document.

References

[1]Waltrup, P., "Liquid-Fueled Supersonic Combustion Ramjets: A Research Perspective," *Journal of Propulsion and Power*, Vol. 3, No. 6, 1987, pp. 515-524.

[2]Holden, M. S., Wieting, A. R., Moselle, J. R., and Glass, C., "Studies of Aerothermal Loads Generated in Regions of Shock/Shock Interaction in Hypersonic Flow," AIAA Paper 88-0477, Jan. 1988.

[3]Yee, H., private communication, Nov. 1989.

[4]Lewis, M. J., and Hastings, D. E., "Bow Shock Matching with Viscous Effects on Hypersonic Forebodies," AIAA Paper 89-2678, July 1989.

[5]Ng, W.-F., "Time Resolved Measurements in a Transonic Compressor Stage," Ph.D. Dissertation, Dept. of Mechanical Engineering, Massachusetts Inst. of Technology, Cambridge, MA, 1983.

[6]Anderson, J. D., *Modern Compressible Flow with Historical Perspective,* McGraw-Hill, New York, 1982, p. 90.

[7]Bertram, M. H., and Blackstock, T. A., "Some Simple Solutions to the Problem of Predicting Boundary-Layer Self-Induced Pressures," NASA TN D-798, April 1961.

[8]Courant, R., and Friedrichs, K. O., *Supersonic Flow and Shock Waves,* Interscience, New York, 1948.

[9]MacCormack, R. W., "The Effect Viscosity in Hypervelocity Impact Catering," AIAA Paper 69-354, Jan. 1969.

[10]Anderson, J. D., *Hypersonic and High Temperature Gas Dynamics,* McGraw-Hill, New York, 1989.

[11]Hung, C. M., and MacCormack, R. W., "Numerical Solutions of Supersonic and Hypersonic Laminar Compression Corner Flows," *AIAA Journal,* Vol. 14, No. 4, 1976, pp. 475-481.

[12]Rogers, C. R., and Schexnayder, C. J., "Chemical Kinetic Analysis of Hydrogen-Air Ignition and Reaction Times," NASA TP-1856, May 1981.

[13]Lewis, M. J., "The Prediction of Inlet Flow Stratification and Its Influence on the Performance of Air-breathing Hypersonic Propulsion Systems," Ph.D. Dissertation, Dept. of Aeronautics and Astronautics, Massachusetts Inst. of Technology, Cambridge, MA, 1988.

[14]Lewis, M. J., and Hastings, D. E., "Some Consequences of Flow Non-Uniformities on the Forebody of a Trans-Atmospheric Vehicle," AIAA Paper 88-3057, July 1988.

Recommended Reading from the AIAA Progress in Astronautics and Aeronautics Series . . . AIAA

Thermal Design of Aeroassisted Orbital Transfer Vehicles

H. F. Nelson, editor

Underscoring the importance of sound thermophysical knowledge in spacecraft design, this volume emphasizes effective use of numerical analysis and presents recent advances and current thinking about the design of aeroassisted orbital transfer vehicles (AOTVs). Its 22 chapters cover flow field analysis, trajectories (including impact of atmospheric uncertainties and viscous interaction effects), thermal protection, and surface effects such as temperature-dependent reaction rate expressions for oxygen recombination; surface-ship equations for low-Reynolds-number multicomponent air flow, rate chemistry in flight regimes, and noncatalytic surfaces for metallic heat shields.

***TO ORDER:* Write, Phone or FAX:**
American Institute of Aeronautics and Astronautics,
c/o TASCO, 9 Jay Gould Ct., P.O. Box 753, Waldorf, MD 20604
Phone (301) 645-5643, Dept. 415 ▪ FAX (301) 843-0159

Sales Tax: CA residents, 7%; DC, 6%. For shipping and handling add $4.75 for 1-4 books (call for rates for higher quanties). Orders under $50.00 must be prepaid. Foreign orders must be prepaid. Please allow 4 weeks for delivery. Prices are subject to change without notice. Returns will be accepted within 15 days.

1985 566 pp., illus. Hardback
ISBN 0-915928-94-9
AIAA Members $54.95
Nonmembers $81.95
Order Number V-96